Applied Catalysis B: Environmental 150–151 (2014) 37–46

Contents lists available at ScienceDirect

Applied Catalysis B: Environmental

journal homepage: www.elsevier.com/locate/apcatb

One-pot glycerol oxidehydration to acrylic acid on multifunctional catalysts: Focus on the influence of the reaction parameters in respect to the catalytic performance

Alessandro Chieregato[a,b,c], M. Dolores Soriano[b], Francesco Basile[a,c], Giuseppe Liosi[a], Segundo Zamora[b], Patricia Concepción[b], Fabrizio Cavani[a,c,*], José M. López Nieto[b,**]

[a] Dipartimento di Chimica Industriale "Toso Montanari", ALMA MATER STUDIORUM Università di Bologna, Viale Risorgimento 4, 40136 Bologna, Italy
[b] Instituto de Tecnología Química, UPV-CSIC, Campus de la Universidad Politécnica de Valencia, Avda. Los Naranjos s/n, 46022 Valencia, Spain
[c] Centro Interdipartimentale di Ricerca Industriale "Energia e Ambiente", Università di Bologna, Bologna, Italy

ARTICLE INFO

Article history:
Received 1 October 2013
Received in revised form
23 November 2013
Accepted 27 November 2013
Available online 6 December 2013

Keywords:
Glycerol
Acrylic acid
Oxidehydration
W–V–Nb mixed oxides
Hexagonal tungsten bronze

ABSTRACT

We report on a study of the key reaction parameters in glycerol oxidehydration into acrylic acid over W–V–Nb mixed oxides with a hexagonal tungsten bronze structure. This investigation demonstrated that the optimal control of the two consecutive steps of acid-catalysed glycerol dehydration into acrolein and aldehyde oxidation into acrylic acid, and of the parallel reaction of acrolein transformation into by-products (ketals and oligomers), was achieved in the presence of a defined glycerol-to-oxygen inlet ratio. Indeed, oxygen played the fundamental role of accelerating the oxidation of the intermediately formed acrolein into acrylic acid, by allowing a greater concentration of the oxidizing V^{5+} sites. In fact, an unprecedented higher yield to acrylic acid and acrolein compared to W–V bronzes was registered (maximum acrylic acid yield 50.5%) together with an increase of more than one order of magnitude in productivity, because of both the greater concentration of glycerol used in the inlet feed and the lower contact time needed. Further experiments were carried out by reacting acrolein and methanol in oxidative conditions, the latter as a model molecule for the determination of surface acid and redox properties.

1. Introduction

With the aim of reducing the carbon footprint of fuels, biodiesel represents one of the most important options, theoretically providing a neutral CO_2 balance and significant reduction in greenhouse gas emission [1–3]. The growing biodiesel production trend goes hand-in-hand with the availability of large volumes of glycerol, co-produced via the conventional transesterification reaction used to synthesize the bio-fuel [2,4]. Since the late 1990s, this abundance of glycerol has significantly impacted the glycerin market, resulting in a lowering of its price [5,6], and making glycerol become a desirable, low-cost raw material for conversion into different chemicals with higher economic value. On the other hand, it must be mentioned that starting in 2007, the glycerin market has faced very volatile conditions, recent price increases, and a supply shortage of refined glycerol [7] which, today, makes difficult any accurate economic evaluation of chemical processes designed for its transformation. However, since the over-supply of crude glycerol from biodiesel production (bio-crude) is one of the main reason for price volatility, the transformation of glycerol toward more added-value products is a key element for developing a new bio-based chemical industry.

Among the several options focused on glycerol conversion, a great deal of attention has been paid to the dehydration of glycerol into acrolein [1,4,7–31], and, more recently, also to the oxidehydration of glycerol into acrylic acid [32–42]. From both the economic and the engineering standpoint, an interesting option for performing the latter reaction is the one-pot (single-step) transformation, by means of a multifunctional catalyst able to carry out both the dehydration of glycerol into acrolein and the aldehyde oxidation into acrylic acid.

Previously we reported that W–V oxides with hexagonal tungsten bronze (HTB) structure and V^{4+} incorporated into a WO_3 lattice are effective catalysts for the direct synthesis of acrylic acid from glycerol [38]; under the best conditions these systems showed 25% acrylic acid yield plus 11% yield to residual acrolein. Later we studied the influence of Nb addition to V-doped HTB structures, with the aim of improving the acidic features of the catalysts so as to

* Corresponding author at: Dipartimento di Chimica Industriale "Toso Montanari", ALMA MATER STUDIORUM Università di Bologna, Viale Risorgimento 4, 40136 Bologna, Italy. Tel.: +39 0512093680.
** Corresponding author. Tel.: +34 963877808.
E-mail addresses: fabrizio.cavani@unibo.it (F. Cavani), jmlopez@itq.upv.es (J.M. López Nieto).

0926-3373/$ – see front matter © 2013 Elsevier B.V. All rights reserved.
http://dx.doi.org/10.1016/j.apcatb.2013.11.045

enhance the glycerol dehydration step. Three-component catalysts (W–V–Nb–O) further increased the catalytic performance, leading in the end to 33% acrylic acid yield plus 17% yield to residual acrolein [41]. Moreover, since the optimum working condition for W–V–Nb–O catalysts is situated at a much lower contact time (from 0.38 s to 0.15 s) than for the W–V–O system, the catalyst productivity was also consistently increased.

In order to fully investigate the catalyst activity of the best-performing tri-component sample (reported as WVNb-1 sample) [41], we report here a complete study of the catalyst behavior as a function of reaction conditions, which enabled us to reach unprecedented values of acrylic acid yield and productivity. Moreover, we also report on the methanol oxidative gas-phase transformation into formaldehyde and dimethyl ether (DME) on both W–V–O and W–V–Nb–O catalysts; indeed, methanol is known to be a suitable probe for exploring the acid and redox properties of metal oxides [45,46]. The results obtained make it possible to draw important general conclusions on the relation between the reaction conditions and catalyst features needed to convert oxygenated molecules by means of direct processes, using a single multifunctional catalyst.

Finally, so as to support the conclusions depicted on HTB doped structures, the same reactions were carried out on Mo–V–(W) oxides with Mo_5O_{14}-type bronze structure. In order to obtain a complete picture of the catalysts behavior, the acrolein oxidation reaction was also studied on both HTBs and Mo_5O_{14}-type bronzes.

2. Experimental

2.1. Synthesis of multicomponent catalysts

The W–V and W–V–Nb catalysts, with HTB structure, were prepared hydrothermally from gels obtained from the aqueous solution of corresponding salts: ammonium metatungstate hydrate (≥85 wt% WO_3 basis, Sigma–Aldrich), vanadium (IV) oxide sulfate hydrate (≥99.99%, Sigma–Aldrich) and niobium oxalate (monooxalate adduct, ABCR), with a W/V and W/V/Nb molar ratio in gel of 1/0.2 and 1/0.2/0.15, respectively. The hydrothermal synthesis was carried out at 175 °C for 48 h. Then the solid was washed and dried at 100 °C overnight. Lastly, the solid was heat-treated in N_2 at 600 °C for 2 h. More details on the preparation have already been reported elsewhere [38,41].

The Mo–V–(W) catalyst, with a Mo_5O_{14} type structure, was prepared from an aqueous solution of ammonium heptamolybdate (GR for analysis, MERCK), vanadium (IV) oxide sulfate hydrate and ammonium metatungstate (with a Mo/V/W molar ratio of 0.68/0.23/0.09), by evaporation in a rotavapor (at 50 °C). The solid was dried at 100 °C overnight and then calcined in air at 350 °C. Lastly, the solid was heat-treated in N_2 at 500 °C for 2 h.

2.2. Catalysts characterization

Surface areas were obtained from N_2 adsorption isotherms using the BET method; a Micromeritics ASAP 2000 instrument was used. Samples were degassed in situ under vacuum at 250 °C.

Powder X-ray diffraction patterns (XRD) were collected using a PANalytical X'Pert PRO diffractometer with CuKα radiation and an X'Celerator detector in Bragg-Brentano geometry.

Scanning electron microscopy (SEM) micrographs were collected in a JEOL 6300 microscope operating at 20 kV, 2×10^{-9} A beam current and 15 mm as working distance. The quantitative EDS analysis was performed using an Oxford LINK ISIS System with the SEMQUANT program, which introduces the ZAF correction. The counting time was 100 s for major and minor elements.

Infrared spectra were recorded at room temperature in the 300–4000 cm^{-1} region with a Nicolet 205xB spectrophotometer equipped with a data station at a spectral resolution of 1 cm^{-1} and accumulations of 128 scans. Raman spectra were obtained with an "in via" Renishaw spectrometer, equipped with an Olympus microscope. The exciting wavelength was 514 nm from a Renishaw HPNIR laser with a power of approximately 15 mW on the sample. The dehydration of catalysts (under 20 mL min^{-1} argon flow at 150 °C) was carried out by using a home-designed microreactor for in situ Raman spectroscopy measurement.

Temperature-programmed reduction (TPR) experiments were carried out on 10–20 mg of catalyst with a N_2:H_2 flow (10% H_2, total flow 50 mL min^{-1}). The temperature range explored was from room temperature to 650 °C. The heating rate was maintained at 10 °C min^{-1}.

Experiments of temperature-programmed desorption of ammonia (TPD) were carried out on a TPD/2900 apparatus from Micromeritics. A 0.30 g sample was pre-treated in a He stream at 450 °C for 1 h. Ammonia was chemisorbed by pulses at 100 °C until equilibrium was reached. Then, the sample was fluxed with a He stream for 15 min, prior to increasing the temperature up to 500 °C in a helium stream of 100 mL min^{-1} and using a heating rate of 10 °C min^{-1}. The NH_3 desorption was monitored with a thermal conductivity detector (TCD) and a mass-spectrometer following the characteristic mass of ammonia at 15 a.m.u.

X-ray photoelectron spectroscopy (XPS) measurements were performed on a SPECS spectrometer equipped with a Phoibos 150 MCD-9 detector using a monochromatic AlKα (1486.6 eV) X-ray source. Spectra were recorded using analyzer pass energy of 50 V, an X-ray power of 200 W, and an operating pressure of 10^{-9} mbar. Spectra treatment was performed using the CASA software. Binding energies (BE) were referenced to C1s at 284.5 eV.

2.3. Reactivity experiments

Reactivity experiments for glycerol, acrolein and methanol transformation were carried out using a continuous flow reactor made of glass, operating at atmospheric pressure. For each condition, all the reaction parameters are always listed in each figure. A catalyst amount ranging from 0.10 to 0.30 g was loaded in powder form. Residence time (calculated as the ratio between catalyst volume (mL) and total gas flow (mL s^{-1}), the latter being measured at room temperature) was varied; for better clarity, the time factor (calculated as the ratio between catalyst mass (g) and total gas flow (mL min^{-1}), the latter being measured at room temperature) was also reported. Inlet feed molar ratios between reactants were also changed according to the desired compositions. If not differently specified, the catalytic results were obtained after 90 min reaction time.

For both glycerol oxidehydration and acrolein oxidation, the effluent stream was bubbled through two in-series abatement devices, which were filled with water (but in some cases anhydrous acetone was used, for the identification of compounds which are less soluble in water) and held at a temperature of 0–2 °C; a third refrigerated condenser was left without any solvent. After this abatement, the gaseous stream, still containing oxygen and carbon oxides, was fed to an automatic sampling system for gas-chromatography (GC-TCD) analysis. The water solution containing the unconverted glycerol and reaction products was analyzed by GC, using a Hewlett-Packard 5890 instrument equipped with a FID detector. A semi-capillary wide-bore OV 351 (polyethyleneglycol treated with terephthalic acid) column was used for the separation of condensed compounds [41]. Two wide-bore columns were used for the separation of non-condensable products: a Molecular sieve 5A for oxygen and CO, and a Silica Plot for CO_2 (oven temperature 80 °C). Compounds were identified by means of both GC–MS and the injection of pure reference standards for the comparison of

Table 1
Main characteristics of fresh samples.

Sample	Surface area ($m^2\ g^{-1}$)	TPD-NH_3		H_2-TPR[a]		Crystalline phase	Catalyst composition[c]
		$\mu mol\ NH_3\ g^{-1}$	$\mu mol\ NH_3\ m^{-2}$	Peak 1	Peak 2		
W–V	19	72	3.8	0.59	2.09	HTB	$WV_{0.14}$
W–V–Nb	57	192	3.4	n.c. [b]	3.99	HTB	$WV_{0.12}Nb_{0.16}$
Mo–V–(W)	6	21	3.5	0.08	2.91	Mo_5O_{14}	$Mo_{0.68}V_{0.23}W_{0.09}$

[a] H_2-TPR results: H_2-uptake (in mmol $H_2\ g^{-1}$) in the 450–550 °C (peak 1) and 550–750 °C (peak 2) temperature region.
[b] The H_2-uptake have been not calculated since only a shoulder is observed at 590 °C for the first reduction peak.
[c] Data calculated by means of SEM–EDX analysis.

retention times in the GC column. A few unknown compounds were eluted in the GC column; we attributed to these compounds the same response factor of the corresponding known compound with the closest retention time. In the figures included with this paper, minor identified products and unknown compounds eluted have been grouped together under the heading "Others". Cyclic ethers were also sometimes produced; however, since with the chromatographic set-up used it was not possible to perfectly resolve each peak correspondent to cyclic ethers, both the latter compounds and heaviest compounds not eluted in the GC column (left as residues on both catalyst surface and reactor walls), were quantified as the lack to the total C balance and labeled as "heavy compounds". Only for catalytic tests where the cyclic ethers presence was found to be more relevant, specific analysis with both GC–MS and ESI-MS was carried out in order to elucidate their nature.

The oxidative transformation of methanol was carried out in a fixed bed reactor at atmospheric pressure in the 250–400 °C temperature region. The catalyst weight was either 0.10 g or 0.20 g, and the feed consisted in a methanol/oxygen/nitrogen mixture with a molar ratio of 6/13/81 (total flow of 100 mL min^{-1}). The analysis of reactants and products was carried out by means of gas-chromatography, using two different chromatographic columns: (i) Molecular sieve 5A (3 m length) and (ii) RT-U-bond (30 m, 0.53 i.d.).

3. Results and discussion

3.1. Characterization of mixed-oxide catalysts

The surface area of the solids synthesized decreased as follows: W–V–Nb > W–V > Mo–V–(W) (Table 1); the difference in surface area can be attributed to both the different structures (the laminar one of Mo–V–(W) being more packed than the W–V–Nb and W–V hexagonal tungsten bronze), and the amount of niobium introduced in the material [41,59,60]. On the other hand, the chemical composition of these materials (determined by EDS microanalysis), revealed a homogeneous distribution of the elements in all cases.

Powder XRD reports of heat-treated materials are presented in Fig. 1. Diffraction maxima match with those of a basic hexagonal tungsten bronze, HTB structure (JCPDS: 85-2460) for W–V and W–V–Nb catalysts, even if, for the latter catalyst, a consistent amount of amorphous phase is present (ca. 60%, calculated by means of the Rietveld method); an analysis concerning the influence of amorphous species in respect to the catalytic performance will be reported elsewhere.

In the case of Mo–V–(W) mixed oxides the line positions and intensities are very similar to those reported previously for catalysts presenting a Mo_5O_{14}-type structure [47–50], i.e., Mo_5O_{14} oxide (JCPDS: 12-0517) or $Nb_{0.09}Mo_{0.91}O_{2.8}$ (JCPDS: 27-1310), having a tetragonal lattice cell. However, the presence of MoO_3 (JCPDS: 5-508), as minority, cannot be completely excluded.

The structure of hexagonal tungsten bronze (i.e., $A_xW^{5+}{}_yW^{6+}{}_{1-y}O_3$ or $A_xM_yW_{1-y}O_3$; where M can be V or Nb and A is typically an electropositive element such as an alkali, alkaline earth or a rare earth but also NH_4^+) can be described as a three dimensional network of corner sharing WO_6 octahedra (or in general MO_6 octahedra) containing hexagonal and trigonal channels along *c* axis, and where the metal ions A, occupy only the hexagonal channels. In our case, in the as-synthesized samples the hexagonal channels are occupied by NH_4^+ cations, which however are eliminated during the heat-treatment in the 400–450 °C temperature interval [38].

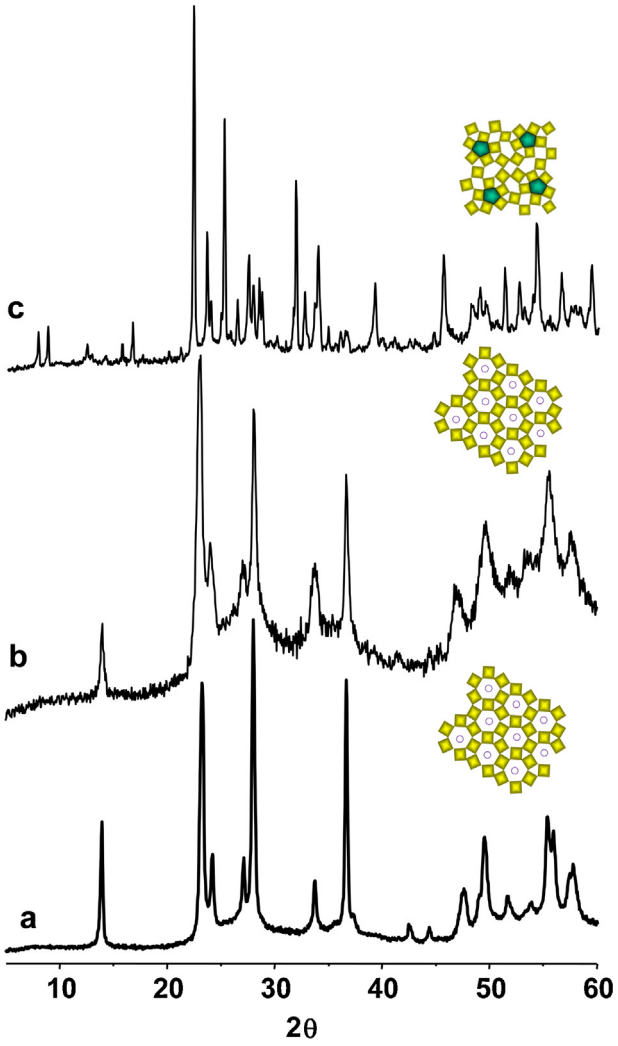

Fig. 1. XRD spectra of the fresh catalysts: (a) W–V, (b) W–V–Nb, (c) Mo–V–(W).

Fig. 2A shows the IR spectra of catalysts. The IR spectrum of W–V and W–V–Nb is very similar presenting a broad band at ca. 802 cm^{-1} (spectrum a) or 828 cm^{-1} (spectrum b), respectively, which can be assigned to O–W–O stretching modes in tungsten oxide with HTB crystal structure [38,41]. Moreover, the broad band in the 700–550 cm^{-1} range can be assigned to W–O–X (X = W, V or Nb) stretching modes [51]. A different IR spectrum is observed in

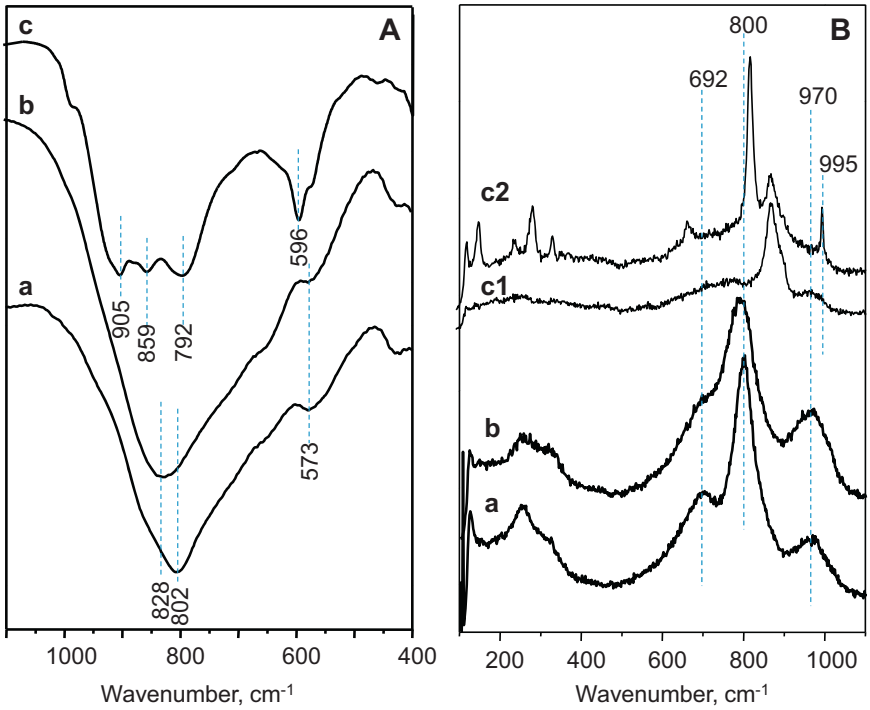

Fig. 2. FTIR spectra (A) and Raman spectra (B) of fresh catalysts: (a) W–V, (b) W–V–Nb, (c) Mo–V–(W).

the case of Mo–V–(W) (spectrum c). Thus, three intense bands are observed at 905, 859 and 792 cm^{-1}, which have also been reported in a Fe-doped Mo/V/W [50] and Ta-containing Mo_5O_{14} [52], both presenting M_5O_{14}-type bronze structure. However, this spectrum is different from that previously reported for Mo- and W-based bronze with a tetragonal tungsten bronze, TTB, structure [53]. On the other hand, the presence of a shoulder at 995 cm^{-1} (as well as low intense bands at 870 and 583 cm^{-1}) suggests the minor presence of MoO_3 [54].

Raman spectra of fresh catalysts are presented in Fig. 2B. The Raman spectra of W–V and W–V–Nb show three broad bands at 970, 800 and 692 cm^{-1}, similar to those previously reported for W-based HTB materials [38,41]. However, in the case of sample Mo–V–(W) (spectra c1 and c2), heterogeneous material is observed as concluded from the different spectra achieved for this sample. The band at ca. 845 cm^{-1} is related to Mo–O bond in Mo_5O_{14} [47]. Moreover, and in addition to Mo_5O_{14}-type crystals, the Raman bands at 673, 822 and 999 cm^{-1} are typical of MoO_3 crystallites (spectrum c2) [55]. These spectra are similar to those previously reported for $(MoVW)_5O_{14}$ mixed oxides [47] and other Mo-based materials presenting Mo_5O_{14}-type structure [48,49], in which the presence of other Mo-oxides, especially MoO_3, is reported.The acid characteristics of catalysts have been investigated by means of TPD of adsorbed ammonia. The NH_3-TPD profiles of catalysts are shown in Fig. 3B and summarized in Table 1. All samples show desorption peaks at approximately 200–220 °C and ca. 350 °C, indicating the presence of both medium and strong acid sites. On the other hand, from the NH_3-desorption profile, in Mo–V–(W) catalyst it is clear the almost complete lack of strong acid sites (with desorption temperature >250 °C) in comparison to both W–V and W–V–Nb samples. Moreover, when considering the number of acid sites per unit weight, W–V–Nb catalyst shows an amount of sites (i.e., 192 μmol NH_3 g^{-1}) higher than in W–V or Mo–V–(W) catalysts. However, when considering the surface area of catalysts, the three samples show a similar density of acid sites, although it decreases as follows: W–V > Mo–V–(W) > W–V–Nb.

Fig. 3A shows the H_2-TPR profiles of catalysts. A small peak is observed for all samples in the 500–600 °C temperature range, which should correspond to the reduction of V-atoms [41]. In addition to this, a peak at high temperature, which shifts depending on the catalyst composition, is also observed. This second peak can be related to the reduction of the rest of elements.

The valence state of constituent elements was studied by XPS. The effect of V loading on the V valence state in W–V–O based catalysts was discussed previously [38,41]. The XPS results are summarized in Table 2, while Fig. 4 shows the V2p and W4f bands. The V/W ratio on the surface of W–V and W–V–Nb mixed oxides (ca. 0.1 and 0.06) is lower to that observed in bulk catalysts (ca. 0.12–0.14 in both samples, Table 1). On the other hand, the W/Mo ratio on the surface of Mo–V–(W) catalyst (ca. 0.15) is similar to that observed in the bulk of catalyst (ca. 0.13, Table 1). However, differences in the oxidation state of each element are observed depending on the catalyst composition. Thus, both V^{4+} (BE = 516.3 eV) and V^{5+} (BE = 517.2 eV) are mainly observed in catalysts, both in fresh and spent ones, except for W–V fresh sample in which the presence of V^{4+} is mainly shown. Moreover, the V^{4+}/V^{5+} ratio on the catalyst surface is higher in Mo–V–(W) catalyst. In the case of tungsten, W^{6+} atoms (in the 35.6–36.2 eV range) are observed in the three catalysts; although, different binding energies were registered, probably as a consequence of different W atoms environment. Nb^{5+} (BE = 206.6 eV, in W–V–Nb) and Mo^{6+} (BE = 232.5 eV, in Mo–V–(W) sample) are the only species observed for these elements.

The presence of Nb^{5+} (i.e., in W–V–Nb) seems to stabilize V^{5+} ions in the fresh sample, which instead is the minor species in the Nb-free catalyst (i.e., in W–V). Moreover, no change in the V^{4+}/V^{5+} ratio of W–V–Nb was observed in the spent catalyst. On the other hand, the presence of V species stabilizes both Mo^{6+} and W^{6+} in Mo–V–(W), as suggested in the case of mixed metal oxides presenting Mo_5O_{14}-type structure, i.e., Mo/Nb/O [49], Mo/V/W/O [47] or Mo/V/Nb/O [48] catalysts.

3.2. Reactivity experiments: oxidehydration of glycerol on W–V–Nb with HTB structure

In order to examine the catalyst activity of the W–V–Nb sample (WVNb-1 in Ref. [41]), the inlet feed composition was changed; for

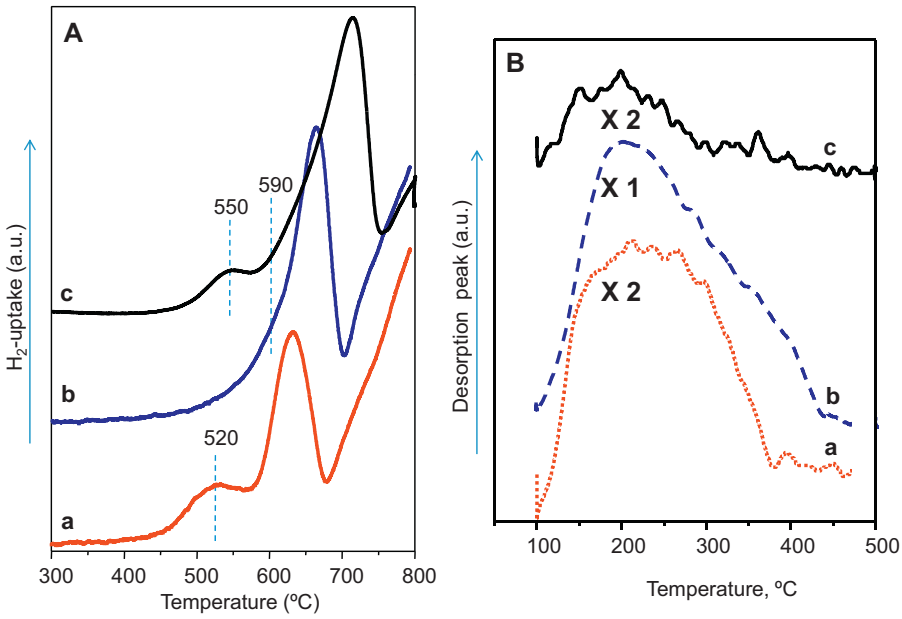

Fig. 3. H_2-TPR patterns (A) and TPD-NH_3 patterns (B) of catalysts: (a) W–V, (b) W–V–Nb, (c) Mo–V–(W).

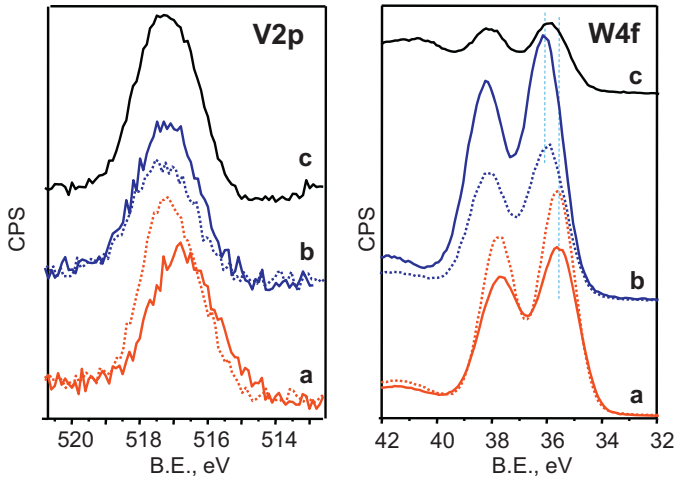

Fig. 4. X-ray photoelectron spectra of V2p and W4f transitions in fresh (continue line) and spent (dashed lines) catalysts: (a) W–V, (b) W–V–Nb, (c) Mo–V–(W).

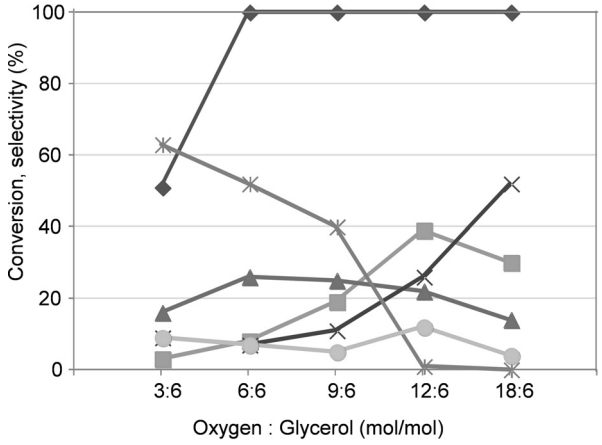

Fig. 5. Glycerol oxidehydration on W–V–Nb catalyst. Variable oxygen-to-glycerol ratio. Glycerol conversion (♦), selectivity to acrolein (▲), acrylic acid (■), CO_x (×), others (●), and heavy compounds (⋆). Others: mainly acetaldehyde and acetic acid (in minor amounts: allylic alcohol, acetone, propionaldehyde, propionic acid and hydroxyacetone). Reaction conditions: temperature 265 °C, 0.3 g of catalyst, contact time 0.15 s, time factor 0.0039 g_{cat} min mL^{-1}. Feed composition (molar %): glycerol 6%, water 40%, oxygen variable, helium up to 100%.

each oxygen-to-glycerol ratio value, the catalytic performance was analyzed in the temperature range 260–410 °C. Specifically, Fig. 5 shows the catalytic results obtained at 265 °C, where the maximum acrylic acid yield was registered (however, analogous trends were obtained for the other temperatures examined). In this experiment both the glycerol molar content in feed (6%) and the water content (40%) were kept constant; oxygen and inert gas (He) molar contents were changed so as to satisfy both the desired feed composition and the pursued residence time. The latter was always set constant to 0.15 s.

When a stoichiometric amount of oxygen and glycerol was fed (molar ratio 3:6), the glycerol conversion was close to 50% and very low selectivity to both acrolein and acrylic acid were registered. On the other hand, selectivity into heavy compounds was very high. When increasing the amount of oxygen, the heavy compound selectivity dropped in favor of selectivity to other products; the acrylic acid selectivity trend showed a peak (39%) with the oxygen-to-glycerol molar ratio 12:6, finally decreasing in favor of carbon oxides with the molar ratio 18:6.

Fig. 6 shows the results of a set of experiments where the oxygen-to-glycerol molar ratio was kept constantly equal to 2, which proved to be the best ratio in Fig. 5, but the inlet molar fraction of reactants was proportionally decreased compared to the 12:6 oxygen-to-glycerol ratio. In spite of the constant optimal ratio between the reactants, heavy compound selectivity increased mainly with lower selectivity to acrylic acid, when the molar fraction of reactants was decreased. This result was the opposite of what might be expected based on the fact that higher reactant loading should facilitate the condensation reaction leading to heavy compounds. This indicates that the most important parameter affecting catalytic behavior is the oxygen partial pressure; higher oxygen contents enhance the oxidation of the intermediately formed acrolein into acrylic acid, thus limiting the undesired formation of acrolein condensation into by-products. When, instead, lower oxygen molar fractions are used, irrespectively of glycerol partial pressure (i.e., at both low and high glycerol partial pressure),

Table 2
XPS results of fresh and used catalysts.

Sample	W4f7/2[a]	V2p3/2[b]			Nb3d5/2[b]	Mo3d5/2[b]		W:V:O:Nb:Mo
	W^{6+}	V^{3+}	V^{4+}	V^{5+}	Nb^{5+}	Mo^{5+}	Mo^{6+}	Surface atomic ratio
W–V (fresh)	35.5 (1.6)	515.5 (7%)	516.7 (93%)	–	–	–	–	28.4:2.7:68.9:0:0
W–V (spent)	35.6 (1.4)	–	516.2 (20%)	517.3 (80%)	–	–	–	29.8:2.9:67.2:0:0
W–V–Nb (fresh)	36.1 (1.6)	–	516.4 (21%)	517.4 (79%)	207.5 (100%)	–	–	27.3:1.7:66.3:4.5:0
W–V–Nb (spent)	36.0 (1.6)	–	516.5 (24.3%)	517.5 (75.7%)	207.5 (100%)	–	–	25.4:2.1:67.7:4.8:0
Mo–V–(W) (fresh)	35.2 (1.6)	–	516.6 (43.4%)	517.6 (56.6%)			233.1 (100%)	3.9:4.4:65.8:0:25.8

[a] In parenthesis the FWHM.
[b] In parenthesis the atomic content for each ion.

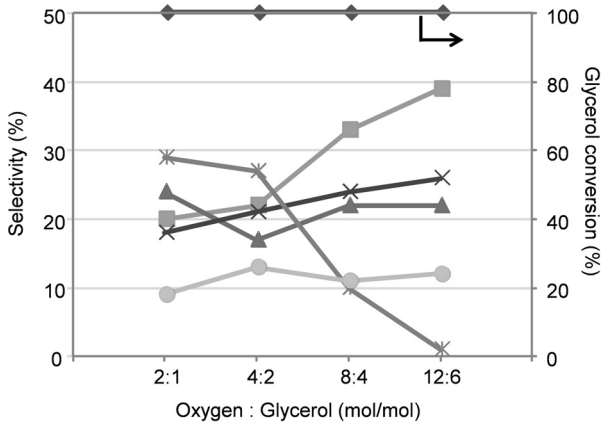

Fig. 6. Glycerol oxidehydration on W–V–Nb catalyst. Constant oxygen-to-glycerol molar ratio (equal to 2). Glycerol conversion (♦), selectivity to acrolein (▲), acrylic acid (■), CO_x (×), others (●), and heavy compounds (⋆). Others: mainly acetaldehyde and acetic acid (in minor amounts: allylic alcohol, acetone, propionaldehyde, propionic acid and hydroxyacetone). Reaction conditions: temperature 265 °C, 0.3 g of catalyst, contact time 0.15 s, time factor 0.0039 g_{cat} min mL^{-1}. Feed composition (molar %): water 40%, glycerol and oxygen variable, helium up to 100%.

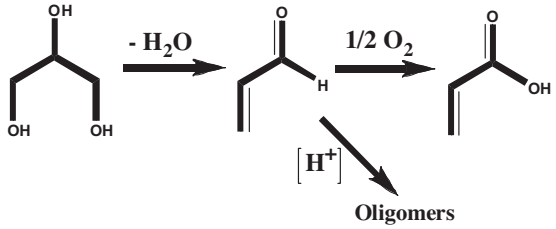

Scheme 1. Competitive reactions in the transformation of the intermediately formed acrolein.

the kinetically preferred reaction involves the transformation of acrolein into by-products (Scheme 1). This strongly suggests that (i) the rate-determining step in the redox mechanism of acrolein transformation into acrylic acid is the oxidation of the reduced V sites into V^{5+}, the latter being the species involved in the aldehyde oxidation; and (ii) the surface concentration of the oxidizing species is thus affected by oxygen partial pressure.

On the other hand, if the partial pressure of oxygen is too high, the selectivity to acrylic acid decreases, with a concomitant increase in carbon oxides (Fig. 5). These findings make it possible to draw an important conclusion: i.e., in order to minimize the undesired competitive reaction of heavier compounds formation – likely catalyzed by the same acid sites which are also required for the glycerol dehydration step – the crucial factor is the development of a steady-state showing a controlled amount of oxidizing sites on the catalyst surface.

Generally speaking, it is important to underline that the reported variations of both acrolein and acrylic acid selectivities might be affected by other unrevealed phenomena masked by the total glycerol conversion; on the other hand, even though conversion is complete, consecutive reactions still are affected by reactants partial pressures and therefore selectivity is also affected.

Fig. 7 compares the productivity into acrolein + acrylic acid for the W–V catalyst [41] and for the W–V–Nb catalyst under non-optimized reaction conditions [38], with the productivity achieved under the conditions shown in the present work, and with results reported in the literature as well. The productivity achieved over W–V–Nb catalyst appeared to be much higher than that previously reported, and also much better than that reported for other catalytic systems and for the two-catalyst in-series reactor configuration, which is the alternative approach proposed in literature.

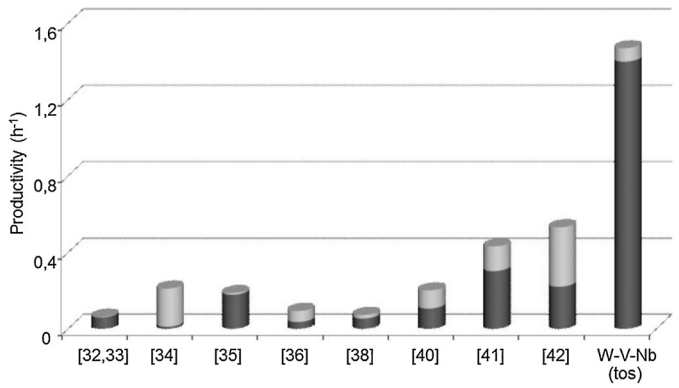

Fig. 7. Comparison of acrylic acid ( ) and acrolein ( ) productivities reported in the literature for glycerol oxidehydration reaction (references in brackets), with the best performance obtained with W–V–Nb catalyst in the time-on-stream test (W–V–Nb tos) reported in this study (acrylic acid yield 50.5%, acrolein yield 3.3%, total glycerol conversion, Fig. 8).

Indeed, the best value achieved, of approximately 1.6 h^{-1}, is quite significant for industrial processes aimed at the synthesis of bulk chemicals or intermediates. It is worth noting that productivity data can differ from those shown if calculated in respect to the specific surface area of the catalysts used (Fig. S-3). On the other hand, from an industrial point of view the relevant parameter to take into account is the productivity as reported in Fig. 7.

3.3. Reactivity experiments: oxidehydration of glycerol on W–V–Nb catalyst, time-on-stream test

Fig. 8(top) shows the catalytic behavior of the W–V–Nb catalyst plotted on the basis of time-on-stream (tos), when using

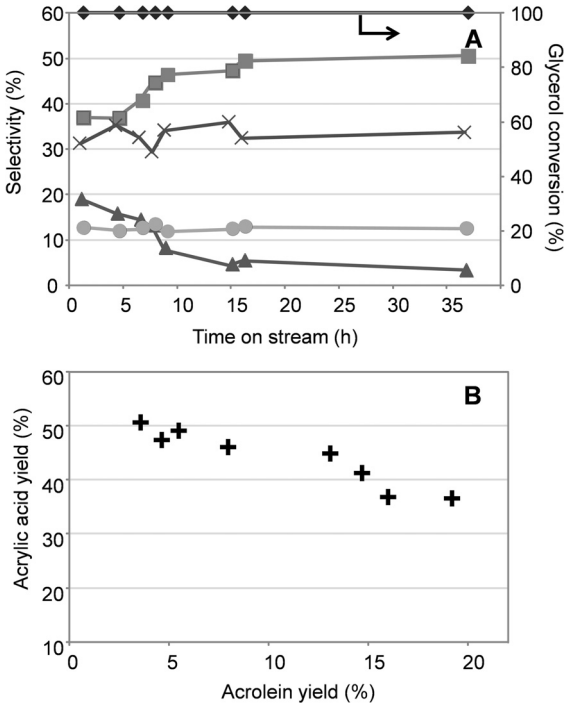

Fig. 8. Glycerol oxidehydration on W–V–Nb catalyst. (A): time-on-stream test. Glycerol conversion (♦), selectivity to acrolein (▲), acrylic acid (■), CO_x (×), and others (●). Others: mainly acetaldehyde and acetic acid (in minor amounts: allylic alcohol, acetone, propionaldehyde, propionic acid and hydroxyacetone). Negligible formation of heavy compounds was registered. Reaction conditions: 0.3 g of catalyst, contact time 0.15 s, time factor 0.0039 g_{cat} min mL^{-1}. Feed composition (molar %): glycerol 6%, oxygen 12%, water 40%, helium 42%. (B): relation between acrolein and acrylic acid yields for all the values observed throughout the time-on-stream test.

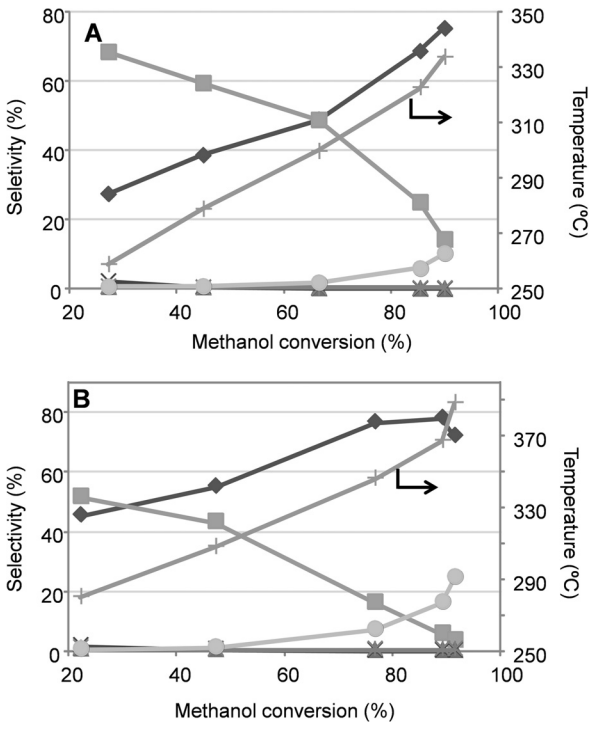

Fig. 9. Oxidative transformation of methanol on W–V–Nb (A) and W–V (B) catalysts. Reaction temperature (+), selectivity to formaldehyde (♦), dimethylether (■), methylformate (▲), dimethoxymethane (×), CO_2 (*), and CO (●). Reaction conditions: 0.1 g of catalyst, contact time 0.06 s, time factor 1×10^{-3} g_{cat} min mL^{-1}. Feed composition (molar %): methanol 6%, oxygen 13%, nitrogen 81%.

experimental conditions that made it possible to obtain the best acrylic acid yield (feed molar ratio O_2/Gly/H_2O/He = 12/6/40/40, temperature 265 °C, residence time 0.15 s). The yields shown in Figs. 5 and 6 were obtained after around 90 min tos, and fit the trends shown here well; on the other hand, after ca. 5 h tos an inverse trend for acrolein and acrylic acid selectivities was registered. Indeed, until around 20 h tos, the consecutive selective oxidation of acrolein to acrylic acid was clearly facilitated, since the acrolein selectivity decreased in favor of acrylic acid. At around 37 h tos, the highest 50.5% acrylic acid yield was registered. Fig. 8(bottom), plotting the yield to both acrolein and acrylic acid registered during experiments shown in Fig. 8(top), demonstrates that a kinetic relationship between acrolein and acrylic acid exists; indeed, the sum of yields to both compounds was always close to 54–55%, even if the relative quantity of the two was consistently different during the time of the experiment.

The XRD analysis on the spent W–V–Nb sample indicates that at the end of the lifetime experiment the catalyst structure was not changed (see XRD pattern of used catalysts in supplementary information, Fig. S-1). In order to elucidate the phenomenon registered, the acid and redox properties of the spent catalyst were analyzed by means of methanol transformation in oxidative conditions, and compared with those of the fresh catalyst. Under the same reaction conditions used in Fig. 9A (vide infra), at low methanol conversion (ca. 28%) the ratio between dimethylether (DME) and formaldehyde (HCHO) yields halved from 2.4 (for the fresh catalyst) to 1.2 (for the catalyst after 37 h of reaction time). This finding is an important evidence that stronger acid sites were neutralized during the lifetime test, most likely due to coking and/or strong adsorption of intermediates or heavy compounds, as highlighted by FTIR spectra of spent catalyst reported in Fig. S-2. Indeed, acid sites can play an important role in the selective oxidation of acrolein into acrylic acid [56].

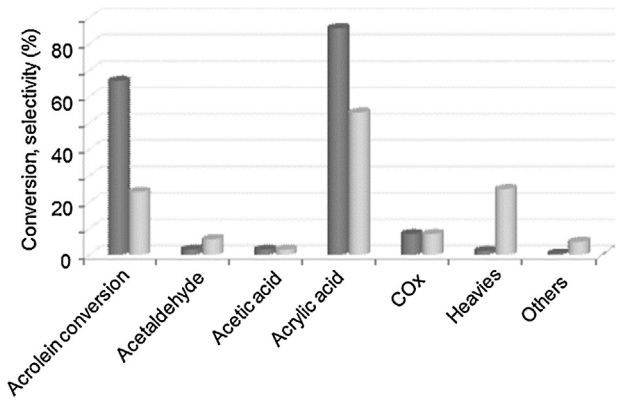

Fig. 10. Acrolein conversion and selectivity to products on W–V–Nb (■) and W–V (□) catalysts. Reaction conditions: 0.3 g of catalyst, contact time 0.15 s, time factor 0.0039 g_{cat} min mL^{-1}. Feed composition (molar %): 2% acrolein, 4% oxygen, 40% water, 54% helium.

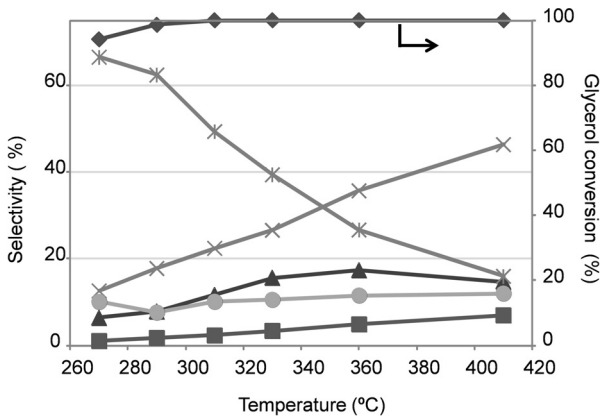

Fig. 11. Glycerol oxidehydration on Mo–V–(W) catalyst. Glycerol conversion (♦), selectivity to acrolein (▲), acrylic acid (■), CO_x (×), others (●), and heavy compounds (*). Others (decreasing order of selectivity): acetaldehyde, acetic acid, allylic alcohol, propionaldehyde, acetone, hydroxyacetone, unknown compounds. Reaction conditions: 0.3 g of catalyst, contact time 0.15 s, time factor 0.0039 g_{cat} min mL^{-1}. Feed composition (molar %): 2% glycerol, 4% oxygen, 40% water, 54% helium.

Moreover, small modifications (due to the presence of different crystalline or amorphous surface structures) during the 5-to-20 h tos cannot be completely ruled out. Indeed, the formation of more active amorphous structures is well known to occur on Mo–V–(W) catalysts – which are similar to those typically used to selectively oxidize acrolein into acrylic acid [44,57,58] – and we cannot rule out the possibility that a similar phenomenon may occur on our W–V–Nb systems.

3.4. Reactivity experiments: reaction with methanol on W–V and W–V–Nb catalysts

Fig. 9A and B shows the results obtained when methanol was made to react in the presence of oxygen on W–V–Nb and W–V catalysts; this latter sample was studied in detail for glycerol oxidehydration in a previous work [38]. As a general trend, at low temperatures the formation of DME was faster than its oxidation into HCHO (higher DME/HCHO ratio); when the temperature was increased, the DME/HCHO ratio decreased. High temperatures led to both decomposition and total oxidation, thus increasing the overall carbon oxide selectivity, mainly carbon monoxide, through HCHO decomposition. Minor amounts of dimethoxymethane and methylformiate also formed.

When comparing the catalytic behavior of W–V and W–V–Nb, it is possible to see that with the latter sample there was a much higher selectivity to DME, in accordance with its higher acid strength. With the increase in temperature, the reaction of methanol oxidehydrogenation to HCHO kinetically prevailed over the etherification reaction; lastly, at high methanol conversion (90%), HCHO selectivity was almost identical for the two catalysts. Moreover, it is interesting to note that different temperatures were needed to achieve similar conversions: for the W–V–Nb catalyst, 90% methanol conversion appeared at 330–335 °C, whereas for the W–V catalyst the same conversion was achieved at 380 °C. This difference is attributable to a higher specific surface area of the Nb-containing sample, which is one of the main features of this catalyst compared to the W–V; moreover, the faster reaction of methanol etherification may also contribute to the higher activity registered. CO selectivity also was slightly different for the two catalysts, respectively, 10% for W–V–Nb and 16% for W–V (at the same methanol conversion of 90%).

3.5. Reactivity experiments: acrolein conversion on W–V and W–V–Nb catalysts

Fig. 10 compares the catalytic results obtained when acrolein was made react on W–V and W–V–Nb catalysts. Under the same working conditions, the two catalysts showed important differences: the W–V sample exhibited both a lower acrolein conversion than W–V–Nb, which again may be explained by taking into account both the higher specific surface area of this latter sample, and a lower selectivity into acrylic acid, with higher selectivity to heavy compounds. Therefore, it may be suggested that the improved acid features of this latter sample may help the desorption of acrylic acid [43], thus limiting its combustion. On the other hand, the low selectivity to acrolein oligomers suggests that the aldehyde oxidation into acrylic acid is much faster than the side acid-catalyzed reactions, which may also be related to the high concentration of V sites. The latter, in turn, is greatly affected by oxygen partial pressure (see above), but a role of Nb ions in facilitating the reoxidation of reduced V sites may not be ruled out.

3.6. Reactivity experiments: comparison with Mo–V–(W) oxide

With the aim of demonstrating the general conclusions drawn on W–V–Nb catalyst, which shows better performance compared to W–V, we report the catalytic results obtained on Mo–V–(W), presenting a mixture of Mo_5O_{14} and MoO_3 although with high Mo_5O_{14}/MoO_3 ratio, which is a model catalyst for the selective oxidation of acrolein into acrylic acid [47,48].

Fig. 11 shows the results obtained in the oxidehydration of glycerol under the same conditions found as optimal for W–V–Nb [41]. As highlighted by the catalyst characterization (NH_3-TPD tests, Fig. 3B), this mixed oxide shows very poor acid properties in terms of acid strength; this finding is reflected very well in the reactivity results of both glycerol (Fig. 11) and methanol (Fig. 12). Indeed, when glycerol was made react on this catalyst, very high selectivity to heavier compounds was registered, since the unconverted glycerol can react with the produced aldehyde to form ketals (cyclic ethers). In fact, if the catalyst does not have the acid properties needed to quickly and selectively dehydrate glycerol into acrolein, the formation of other by-products is detected, e.g., cyclic ethers such as 1,3-dioxan-5-ol and 1,3-dioxolan-4-yl-methanol, formed by the reaction between glycerol and formaldehyde or acetaldehyde, the latter compounds being in turn formed by the retro-aldol condensation of 3-hydroxypropanal, one product of glycerol mono-dehydration [35]. The intermediately formed acrolein may react in a similar way with glycerol to form other cyclic ethers, as shown in Scheme 2; indeed, the formation of these ethers was confirmed by means of ESI-MS analysis of the reaction mixture.

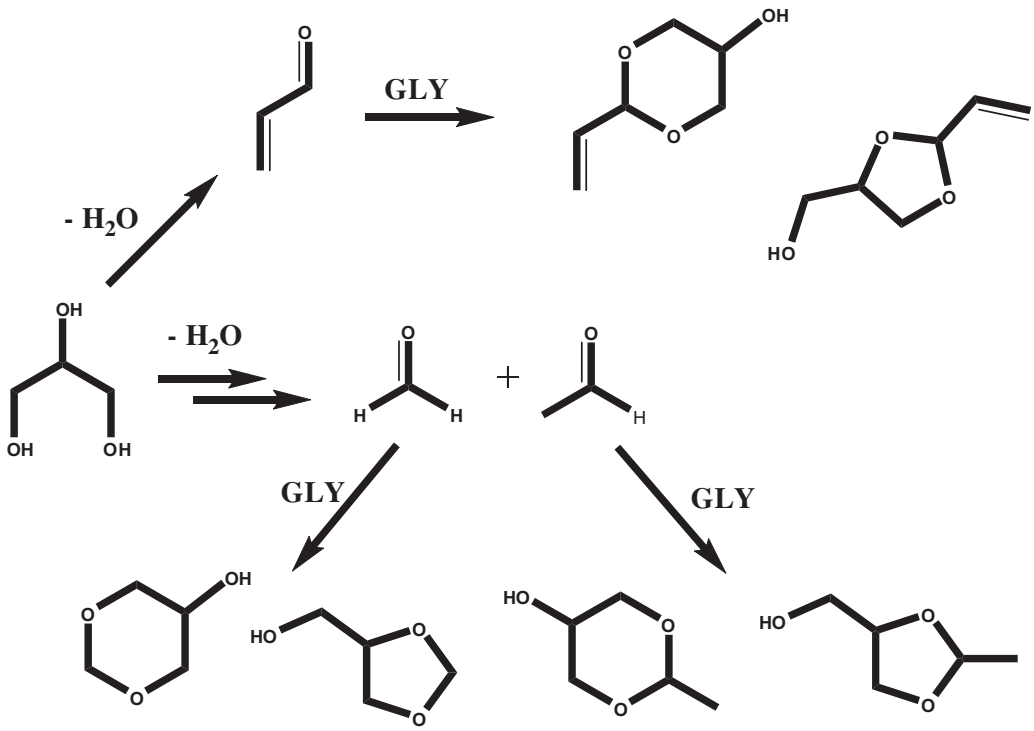

Scheme 2. Ketals formation pathways as by-products of the glycerol oxidehydration reaction.

When the temperature was raised, the ketal selectivity decreased mainly in favor of CO_x and acrolein formation; on the other hand, the acrylic acid selectivity remained low, even if the catalyst is specifically designed for acrolein oxidation into acrylic acid. When acrolein was fed in analogous conditions (residence time 0.15 s, temperature 360 °C), selectivity to acrylic acid was close to 70% at 20% acrolein conversion. This was apparently due to both the low selectivity to acrolein and the specific residence time used (optimal for glycerol dehydration on W–V–Nb sample with HTB structure), which is too low to convert acrolein into acrylic acid on Mo–V–(W) with Mo_5O_{14}-type structure [47,48].

As already reported for glycerol oxidehydration, the lack of strong acid sites in Mo_5O_{14}-type bronze, Mo–V–(W), is also evident from the catalytic behavior shown in methanol oxidation (Fig. 12); indeed, the acid-catalyzed route to DME was very low.

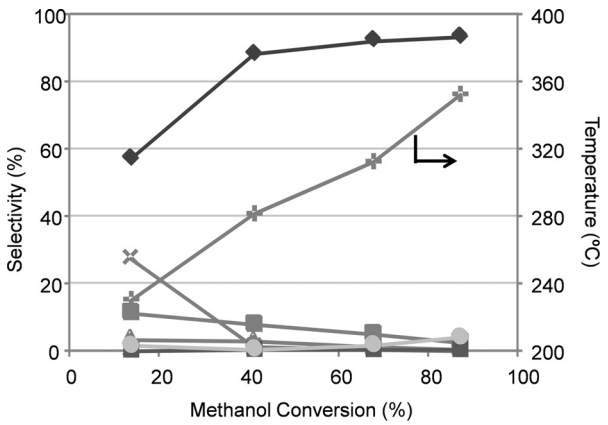

Fig. 12. Oxidative transformation of methanol on Mo–V–(W) catalyst. Reaction temperature (+), selectivity to formaldehyde (♦), dimethylether (■), methylformate (▲), dimethoxymethane (×), CO_2 (*), and CO (●). Reaction conditions: 0.2 g of catalyst, contact time 0.12 s, time factor 2×10^{-3} g_{cat} min mL^{-1}. Feed composition (molar %): methanol 6%, oxygen 13%, nitrogen 81%.

On the other hand, this system proved to be very selective in the oxidation of methanol to HCHO: a maximum aldehyde selectivity equal to 93% was registered at 87% methanol conversion (at 350 °C). These results are similar to those reported over a Fe-doped Mo/V/W mixed oxides with similar both catalyst composition and crystalline phase [50]. At low temperatures, we also observed the formation of dimethoxymethane, which may derive from the acetalization of HCHO with the unconverted methanol. On the other hand, because of the low specific surface area of this catalyst, in order to obtain methanol conversions close to those obtained by both W–V and W–V–Nb catalysts, higher contact time (0.12 s) was needed, as compared to that used with the latter systems (0.06 s).

4. Conclusions

The studies carried out on both HTBs and Mo_5O_{14}-type oxides have led us to draw important conclusions on the relation between reaction conditions and catalyst features needed by multifunctional oxides for one-pot oxidehydration starting from glycerol, and more in general from oxygenated compounds. Indeed, the consecutive oxidation step must be fast, compared to the dehydration step, in order to avoid the formation of heavy compounds generated by both ketal formation and oligomerization reactions that take place from the intermediately formed unsaturated aldehyde. For this reason, the latter being achieved by using oxygen partial pressures well above that needed for the stoichiometric oxidehydration of glycerol into acrylic acid, strongly oxidizing conditions are necessary with the best-performing W–V–Nb catalyst. The latter is characterized by high surface area and high concentration of stronger acid sites, properties which on the one hand are important for an efficient dehydration of glycerol into acrolein, but on the other hand might lead to the formation of undesired by-products. Under selected reaction conditions, an outstanding productivity to acrolein + acrylic acid close to 1.6 h^{-1} with a yield to acrylic acid as high as 50.5% were achieved.

Acknowledgements

CIRI (Centro per la Ricerca Industriale), Università di Bologna, is acknowledged for the grant to A.C. The Valencia group also thanks the financial support of Dirección General de Investigación Científica y Técnica in Spain (Project CTQ2012-37925-C03-01).

Appendix A. Supplementary data

Supplementary data associated with this article can be found, in the online version, at http://dx.doi.org/10.1016/j.apcatb.2013.11.045.

References

[1] B. Katryniok, S. Paul, V. Belliere-Baca, P. Rey, F. Dumeignil, Green Chem. 12 (2010) 2079–2098.
[2] P. Pin Oh, H.L. Nang Lau, J. Chen, M. Fong Chong, Y. May Choo, Renew. Sust. Energ. Rev. 16 (2012) 5131–5145.
[3] E. Atabani, A.S. Silitonga, I. Anjum Badruddin, T.M.I. Mahlia, H.H. Masjuki, S. Mekhilef, Renew. Sust. Energ. Rev. 16 (2012) 2070–2093.
[4] B. Katryniok, S. Paul, M. Capron, F. Dumeignil, ChemSusChem 2 (2009) 719–730.
[5] J.A. Kenar, Lipid Techn. 19 (2007) 249–253.
[6] J.M. Clomburg, R. Gonzalez, Trends Biotechnol. 31 (2013) 20–28.
[7] M. Ayoub, A.Z. Abdullah, Renew. Sust. Energ. Rev. 16 (2012) 2671–2686.
[8] A. Martin, U. Armbruster, H. Atia, Eur. J. Lipid Sci. Technol. 114 (2012) 10–23.
[9] H. Atia, U. Armbruster, A. Martin, J. Catal. 258 (2008) 71–82.
[10] H. Atia, U. Armbruster, A. Martin, Appl. Catal. A 393 (2011) 331–339.
[11] S. Erfle, U. Armbruster, U. Bentrup, A. Martin, A. Brückner, Appl. Catal. A 391 (2011) 102–109.
[12] B. Katryniok, S. Paul, M. Capron, C. Lancelot, V. Bellière-Baca, P. Rey, F. Dumeignil, Green Chem. 12 (2010) 1922–1925.
[13] S.-H. Chai, H.-P. Wang, Y. Liang, B.-Q. Xu, J. Catal. 250 (2007) 342–349.
[14] S.-H. Chai, H.-P. Wang, Y. Liang, B.-Q. Xu, Green Chem. 10 (2008) 1087–1093.
[15] S.-H. Chai, H.-P. Wang, Y. Liang, B.-Q. Xu, Appl. Catal. A 353 (2009) 213–222.
[16] A. Ulgen, W.F. Hoelderich, Catal. Lett. 131 (2009) 122–128.
[17] A. Ulgen, W.F. Hoelderich, Appl. Catal. A 400 (2011) 34–38.
[18] C.-J. Jia, Y. Liu, W. Schmidt, A.-H. Lu, F. Schüth, J. Catal. 269 (2010) 71–79.
[19] A. Corma, G.W. Huber, L. Sauvanaud, P. O'Connor, J. Catal. 257 (2008) 163–171.
[20] Y.T. Kim, K.-D. Jung, E. Duck Park, Microp. Mesop. Mater. 131 (2010) 28.
[21] Y.T. Kim, K.-D. Jung, E. Duck Park, Appl. Catal. A 393 (2011) 275–287.
[22] E. Tsukuda, S. Sato, R. Takahashi, T. Sodesawa, Catal. Commun. 8 (2007) 1349–1353.
[23] Q. Liu, Z. Zhang, Y. Du, J. Li, X. Yang, Catal. Lett. 127 (2009) 419–428.
[24] W. Suprun, M. Lutecki, T. Haber, H. Papp, J. Mol. Catal. A 309 (2009) 71–78.
[25] W. Suprun, M. Lutecki, R. Gläser, H. Papp, J. Mol. Catal. A 91 (2011) 342–343.
[26] B. Rafii Sereshki, S.-J. Balan, G.S. Patience, J.-L. Dubois, Ind. Eng. Chem. Res. 49 (2010) 1050–1056.
[27] F. Cavani, S. Guidetti, L. Marinelli, M. Piccinini, E. Ghedini, M. Signoretto, Appl. Catal. B 100 (2010) 197–204.
[28] F. Cavani, S. Guidetti, C. Trevisanut, E. Ghedini, M. Signoretto, Appl. Catal. A 409–410 (2011) 258–267.
[29] P. Lauriol-Garbay, J.M.M. Millet, S. Loridant, V. Bellière-Baca, P. Rey, J. Catal. 280 (2011) 68–76.
[30] P. Lauriol-Garbey, G. Postole, S. Loridant, A. Auroux, V. Belliere-Baca, P. Rey, J.M.M. Millet, Appl. Catal. B 106 (2011) 94–102.
[31] L. Ning, Y. Ding, W. Chen, L. Gong, R. Lin, Y. Li, Q. Xin, Chin. J. Catal. 29 (2008) 212–214.
[32] J.L. Dubois, C. Duquenne, W. Hölderich, Eur. Patent 1874720, 2006, assigned to Arkema France.
[33] J.L. Dubois, WO Patent, 2007/090991; WO Patent, 2008/007002, assigned to Arkema France.
[34] F. Wang, J.-L. Dubois, W. Ueda, J. Catal. 268 (2009) 260–267.
[35] F. Wang, J. Deleplanque, J.-L. Dubois, J.-F. Devaux, W. Ueda, Catal. Today 157 (2010) 351–358.
[36] J. Xu, J.-L. Dubois, W. Ueda, ChemSusChem 3 (2010) 1383–1389.
[37] F. Wang, J.-L. Dubois, W. Ueda, Appl. Catal. A 376 (2010) 25–32.
[38] M.D. Soriano, P. Concepción, J.M. López Nieto, F. Cavani, S. Guidetti, C. Trevisanut, Green Chem. 13 (2011) 2954–2962.
[39] N. Böhmer, T. Roussière, M. Kuba, S.A. Schunk, Comb. Chem. High Throughput Screen 15 (2012) 123–135.
[40] A. Witsuthammakul, T. Sooknoi, Appl. Catal. A 413–414 (2012) 109–116.
[41] A. Chieregato, F. Basile, P. Concepción, S. Guidetti, G. Liosi, M.D. Soriano, C. Trevisanut, F. Cavani, J.M. López Nieto, Catal. Today 197 (2012) 58–65.
[42] C.F.M. Pestana, A.C.O. Guerra, B.F. Glaucio, C.C. Turci, C.J.A. Mota, J. Braz. Chem. Soc. 24 (2013) 100–105.
[43] J. Tichy, Appl. Catal. A 157 (1997) 363–385.
[44] P. Kampe, L. Giebeler, D. Samuelis, J. Kunert, A. Drochner, F. Haaß, A.H. Adams, J. Ott, S. Endres, G. Schimanke, T. Buhrmester, M. Martin, H. Fuess, H. Vogel, Phys. Chem. Chem. Phys. 9 (2007) 3577–3589.
[45] J.M. Tatibouët, Appl. Catal. A 148 (1997) 213–439.
[46] M. Badlani, I.E. Wachs, Catal. Lett. 75 (2001) 137–149.
[47] S. Knobl, G.A. Zenkovets, G.N. Kryukova, O. Ovsitser, D. Niemeyer, R. Schlögl, G. Mestl, J. Catal. 215 (2003) 177–187.
[48] T.Yu. Kardash, L.M. Plyasova, V.M. Bondareva, T.V. Andrushkevich, L.S. Dovlitova, A.I. Ischenko, A.I. Nizovskii, A.V. Kalinkin, Appl. Catal. A 375 (2010) 26–36.
[49] P. Afanasiev, J. Phys. Chem. B 109 (2005) 18293–18300.
[50] B.R. Bhat, J.-S. Choi, T.-H. Kim, Catal. Lett. 117 (2007) 136–149.
[51] C.B. Rodella, P.A.P. Nascente, V.R. Mastelaro, M.R. Zucchi, R.W.A. Franco, C.J. Magon, P. Donoso, A.O. Florentino, J. Vac. Sci. Technol. A 19 (2001) 1158–1163.
[52] F. Cariati, J.C.J. Bart, A. Sgamellotti, Inorg. Chim. Acta 48 (1981) 97–103.
[53] P. Botella, B. Solsona, J.M. López Nieto, P. Concepción, J.L. Jordá, M.T. Doménech-Carbó, Catal. Today 158 (2010) 162–169.
[54] G. Petrini, J.C.J. Bart, Z. Anorg. Allg. Chem. 474 (1981) 229–232.
[55] G. Mestl, T.K.K. Srinivasan, Catal. Rev. Sci. Eng. 40 (1998) 451–570.
[56] T. Jekewitz, N. Blickhan, S. Endres, A. Drochner, H. Vogel, Catal. Commun. 20 (2012) 25–28.
[57] S. Endres, P. Kampe, J. Kunert, A. Drochner, H. Vogel, Appl. Catal. A 325 (2007) 237–243.
[58] L. Giebeler, P. Kampe, A. Wirth, A.H. Adams, J. Kunert, H. Fuess, H. Vogel, J. Mol. Catal. A 259 (2006) 309–318.
[59] P. Botella, B. Solsonaa, J.M. López Nieto, P. Concepción, J.L. Jordáa, M. Teresa Doménech-Carbóc, Catal. Today 158 (2010) 162–169.
[60] N. Blanch-Raga, M.D. Soriano, A.E. Palomares, P. Concepcion, J. Martinez-Triguero, J.M. Lopez Nieto, Appl. Catal. B 130-131 (2013) 36–43.